Inertial oscillations in a confined monopolar vortex subjected to background rotation

Inertial oscillations in a confined monopolar vortex subjected to background rotation

M. Duran-Matute,[a] L. P. J. Kamp, R. R. Trieling, and G. J. F. van Heijst
Department of Applied Physics and J.M. Burgerscentre, Eindhoven University of Technology, P.O. Box 513, 5600 MB Eindhoven, The Netherlands

(Received 8 December 2008; accepted 18 September 2009; published online 11 November 2009)

We study the axisymmetric inertial oscillations in a confined monopolar vortex under the influence of background rotation. By first focusing on the inviscid linear dynamics, and later studying the effects of viscosity and of a no-slip bottom, we characterize the effects of rotation and confinement. It was found that background rotation allows for oscillations outside the vortex core even with frequencies larger than 2Ω, with Ω the background rotation rate. However, confinement is necessary for the system to sustain oscillations with frequencies smaller than 2Ω. Through the analytical solution for a small perturbation of a Rankine vortex, we obtain five regimes where the oscillations are qualitatively different, depending on their frequency. Numerical results for the linear inviscid waves sustained by a Lamb–Oseen vortex show a similar behavior. The effects of viscosity are twofold: the oscillations are damped and the vortex sustaining the oscillations is modified. When a no-slip bottom is considered, a boundary layer drives a secondary motion superimposed on the inertial oscillations. In this case, the vortex is quickly damped, but the oscillations persist due to the background rotation. © *2009 American Institute of Physics*. [doi:10.1063/1.3258670]

I. INTRODUCTION

It has been long known that vortices and flows in solid body rotation sustain inertial oscillations (Kelvin waves).[1] However, such oscillations continue to be a topic of interest due to their importance in the evolution of vortices. In geophysical fluid dynamics, the inertial oscillations in vortices affected by background rotation are of particular interest since such flows are common in both the ocean and the atmosphere (e.g., hurricanes and oceanic eddies).

Following the paper by Lord Kelvin,[1] inertial oscillations have been observed in, for example, experiments on vortices in a turbulent flow[2] and in rotating fluids.[3] Furthermore, several analytical and numerical studies concerning inertial oscillations on vortices with different vorticity structures, both with and without background rotation, have been carried out.

The vortex analyzed by Lord Kelvin—now termed *Rankine vortex*—is composed of a core of uniform vorticity and an exterior with zero vorticity. Due to its shape the stability of a vortex with this profile is easily treated analytically. A formal solution to the initial value problem for small perturbations in a Rankine vortex has shown that any initial perturbation evolves exclusively as a collection of Kelvin waves, and that the physical mechanism of the propagation of the perturbations does not depend on the vortex profile.[4]

Among other vortices studied, the Lamb–Oseen vortex has received special attention due to its similarity to vortices generated in the laboratory, although its profile does not allow a complete analytical solution of the perturbed vortex. However, an exhaustive overview of the modes present in a Lamb–Oseen vortex has been obtained with the help of numerical simulations.[5] Some of the modes turned out to be related to those existing in the Rankine vortex, while others are singular damped modes. Furthermore, a large axial-wave-number approximation has provided the spatial structure and the dispersion relation of the Kelvin modes, with a good agreement with the numerical computation—even for small wave numbers.[6]

The axisymmetric modes form a special case since they are regular modes in a Lamb–Oseen vortex.[5,7] Consequently, their dynamics are similar in both the Rankine vortex and the Lamb–Oseen vortex. The physical mechanism of these axisymmetric modes can be described as follows. Initially, the perturbed vortex consists of regions of high and low vorticity. Because of conservation of angular momentum, the vortex radius is smaller in the regions of high vorticity and larger in the regions of low vorticity (hence the term *sausaging modes*[8]). This shape is associated with alternating high and low pressure perturbations. Therefore, a net axial pressure gradient exists within the core and induces an axial flow. Finally, the axial flow within the vortex affects the axial vorticity through the stretching-compressing mechanism. Consequently, the vortex column undergoes deformations with the varicose shape being reversed repeatedly.[5] An alternative explanation, based on the twisting of the vortex lines, was proposed by Melander and Hussain.[9]

Axisymmetric modes can affect the evolution of vortices. For instance, sausage modes can travel along the vortex and cause it to break down if the vortex is centrifugally unstable. These modes appear even if the vortex column is perturbed in a nonaxisymmetric way.[10,11] However, the Lamb–Oseen vortex, for example, is known to be stable to centrifugal instability, except in the case of strong anticyclones.[12]

The main aim of this paper is to extend the study of the

[a]Electronic mail: m.duran.matute@tue.nl.

oscillations inside the vortex by including the effects of both background rotation and confinement of the fluid to a cylinder of finite dimensions. As mentioned earlier, background rotation is relevant in the study of geophysical flows. On the other hand, confinement is always necessary to contain the fluid.

We restrict our study to a monopolar vortex (swirl flow) and to the axisymmetric inertial oscillations associated with it. We focus on the spatial structure and the frequency of the different modes, as well as on the effect that these modes have on the evolution of the vortex.

Le Dizès[13] performed an extensive study on the inviscid waves on a Lamb–Oseen vortex with background rotation using a local Lagrangian description and a global Wentzel–Kramers–Brillouin–Jeffreys (WKBJ) approach. He found that the global modes exist in more restricted parameter regimes compared with the local approach. Nonetheless, we will show here that this finding is only valid in an infinite domain.

In order to characterize the waves sustained inside monopolar vortices in laboratory experiments and other real settings, we first study the inviscid modes sustained by a time-independent Rankine vortex confined to a cylinder with stress-free boundaries and subjected to background rotation. Second, we study the inviscid waves sustained by a more realistic vortex profile, namely, the Lamb–Oseen vortex. Later, the effects of viscosity are included, and finally, the effects of a no-slip bottom are considered.

The paper is organized as follows. In Sec. II, we introduce the geometry and the nondimensional parameters relevant to the problem. Section III presents the governing equations. In Sec. IV, we analyze the inviscid linear waves, while in Sec. V, we discuss the effects of viscosity including a study of the evolution of the inertial waves in a cylinder with a no-slip bottom (Sec. V B). Finally, in Sec. VI the main results and conclusions are outlined.

II. DEFINITION OF THE PROBLEM

We consider the fluid motion relative to the system rotating at a constant rate Ω about the vertical axis. The relative flow is governed by the Navier–Stokes equation

$$\frac{D\boldsymbol{v}}{Dt} = -\frac{1}{\rho}\boldsymbol{\nabla} P + \nu\nabla^2\boldsymbol{v} - 2\boldsymbol{\Omega}\times\boldsymbol{v} \tag{1}$$

and the continuity equation for an incompressible fluid

$$\boldsymbol{\nabla}\cdot\boldsymbol{v} = 0, \tag{2}$$

where D/Dt is the material derivative, $\boldsymbol{\Omega}=\Omega\hat{\boldsymbol{z}}$ is the rotation vector of the system, $\boldsymbol{v}$ is the relative velocity, P is the generalized pressure, and ρ is the density of the fluid. The motion of the fluid is described in terms of the radial, azimuthal, and axial coordinates (r,θ,z) with unit vectors $\hat{\boldsymbol{r}}$, $\hat{\boldsymbol{\theta}}$, and $\hat{\boldsymbol{z}}$ in these directions. The velocity and vorticity vectors can then be written as $\boldsymbol{v}=(v_r,v_\theta,v_z)$ and $\boldsymbol{\omega}=(\omega_r,\omega_\theta,\omega_z)$, respectively.

The flow studied consists of a vortex with peak vertical vorticity $\hat{\omega}$ and radius L confined to a cylindrical domain with height H and radius L_c, as shown in Fig. 1. The cylinder rotates around the vertical axis with angular frequency Ω.

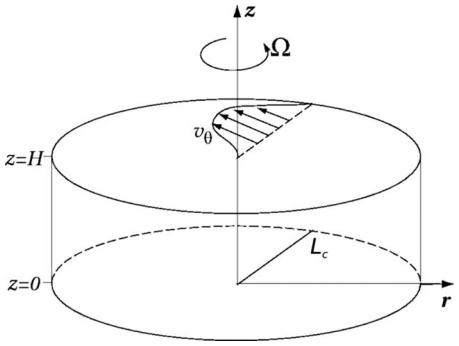

FIG. 1. Schematic representation of the problem.

We consider all boundaries to be stress-free. (Later, in Sec. V B, we will consider the case of a no-slip bottom.) In addition, both the bottom (at $z=0$) and the surface (at $z=H$) are flat and rigid.

Considering the parameters of the problem and performing dimensional analysis yields four nondimensional numbers that describe the problem

$$\mathrm{Ro} = \frac{\hat{\omega}_0}{2\Omega}, \quad \mathrm{Re} = \frac{L_0^2|\hat{\omega}_0|}{\nu}, \quad \delta = \frac{H}{L_0}, \quad \mathrm{R_c} = \frac{L_c}{L_0},$$

where ν is the kinematic viscosity of the fluid, $\hat{\omega}_0$ is the initial peak vorticity of the vortex, L_0 is the initial radius of the vortex, Ro is the Rossby number, Re is the Reynolds number, δ is the aspect ratio of the vortex, and $\mathrm{R_c}$ is the radius of the cylinder compared with the radius of the vortex.

III. THE GOVERNING EQUATIONS

To nondimensionalize Eqs. (1) and (2), the following set of dimensionless variables is defined:

$$t' = |2\Omega + \hat{\omega}_0|t, \quad r' = \frac{r}{L_0}, \quad z' = \frac{z}{H},$$

$$v_r' = \frac{v_r}{\hat{\omega}_0 L_0}, \quad v_\theta' = \frac{v_\theta}{\hat{\omega}_0 L_0}, \quad v_z' = \frac{v_z}{\hat{\omega}_0 H},$$

with the primes denoting nondimensional quantities. By assuming that the flow has azimuthal symmetry, we can write the governing equations in terms of ω_θ' and v_θ' in the following form:

$$\mathrm{N}\frac{\partial v_\theta'}{\partial t'} + \left(v_r'\frac{\partial v_\theta'}{\partial r'} + v_z'\frac{\partial v_\theta'}{\partial z'} + \frac{v_\theta' v_r'}{r'}\right) = -\frac{1}{\mathrm{Ro}}v_r' + \frac{1}{\mathrm{Re}}\left(\frac{\partial^2 v_\theta'}{\partial r'^2} + \frac{1}{r'}\frac{\partial v_\theta'}{\partial r} - \frac{v_\theta'}{r'^2}\right) + \frac{1}{\mathrm{Re}\,\delta^2}\frac{\partial^2 v_\theta'}{\partial z'^2}, \tag{3}$$

$$\mathrm{N}\frac{\partial \omega_\theta'}{\partial t'} + \left(v_r' \frac{\partial \omega_\theta'}{\partial r'} + v_z' \frac{\partial \omega_\theta'}{\partial z'} - \frac{\omega_\theta' v_r'}{r'} - \frac{1}{\delta r'} \frac{\partial v_\theta'^2}{\partial z'} \right) = \frac{1}{\delta\,\mathrm{Ro}} \frac{\partial v_\theta'}{\partial z'} + \frac{1}{\mathrm{Re}} \left(\frac{\partial^2 \omega_\theta'}{\partial r'^2} + \frac{1}{r'} \frac{\partial \omega_\theta'}{\partial r'} - \frac{\omega_\theta'}{r'^2} \right) + \frac{1}{\mathrm{Re}\,\delta^2} \frac{\partial^2 \omega_\theta'}{\partial z'^2}, \tag{4}$$

$$\frac{1}{r'} \frac{\partial}{\partial r'} (r' v_r') + \frac{\partial v_z'}{\partial z'} = 0, \tag{5}$$

with the rotation number $\mathrm{N} = |2\Omega + \hat{\omega}_0| / |\hat{\omega}_0| = |1 + \mathrm{Ro}| / |\mathrm{Ro}|$.

The typical time scale is taken as $|2\Omega + \hat{\omega}_0|^{-1}$, since $|2\Omega + \hat{\omega}_0|$ is the natural rotation frequency at the center of the vortex. Due to this definition of the typical time scale, the correct form of the equations is recovered when $\mathrm{Ro} = \infty$. In this case, the three remaining nondimensional parameters are Re, δ, and $\mathrm{R_c}$. In addition, by multiplying Eqs. (3) and (4) by Ro and making $\hat{\omega}_0 = 0$, we recover the equations for the limit of solid body rotation.

For convenience of notation, the primes will be omitted from here on. Furthermore, it is useful to define the new variables

$$\Phi = \omega_\theta / r \tag{6}$$

and

$$V = r v_\theta + r^2/(2\,\mathrm{Ro}), \tag{7}$$

where V is the absolute angular momentum nondimensionalized with $\hat{\omega}_0 L_0^2$. The system of governing equations can now be written as

$$\mathrm{N}\frac{\partial V}{\partial t} + \frac{1}{r}[V, \psi] = \frac{1}{\mathrm{Re}} \left(r \frac{\partial}{\partial r} \frac{1}{r} \frac{\partial V}{\partial r} \right) + \frac{1}{\mathrm{Re}\,\delta^2} \frac{\partial^2 V}{\partial z^2}, \tag{8}$$

$$\mathrm{N}\frac{\partial \Phi}{\partial t} + \frac{1}{r}[\Phi, \psi] = \frac{1}{\delta r^4} \frac{\partial V^2}{\partial z} + \frac{1}{\mathrm{Re}} \left(\frac{\partial^2 \Phi}{\partial r^2} + \frac{3}{r} \frac{\partial \Phi}{\partial r} \right) + \frac{1}{\mathrm{Re}\,\delta^2} \frac{\partial^2 \Phi}{\partial z^2}, \tag{9}$$

$$\Phi = \frac{1}{r^2} \tilde{\Delta} \psi = \frac{1}{r^2} \left(\delta \frac{\partial^2 \psi}{\partial r^2} - \delta \frac{1}{r} \frac{\partial \psi}{\partial r} + \frac{1}{\delta} \frac{\partial^2 \psi}{\partial z^2} \right), \tag{10}$$

where

$$[f, g] = \frac{\partial f}{\partial r} \frac{\partial g}{\partial z} - \frac{\partial f}{\partial z} \frac{\partial g}{\partial r}, \tag{11}$$

$\tilde{\Delta}$ is the dimensionless modified Laplacian operator, and ψ is the streamfunction defined by

$$v_r = \frac{1}{r} \frac{\partial \psi}{\partial z}, \quad v_z = -\frac{1}{r} \frac{\partial \psi}{\partial r}. \tag{12}$$

Equation (8) shows that for the inviscid case the angular momentum of the fluid is modified exclusively by the meridional flow (v_r, v_z), while Eq. (9) shows that the meridional flow is coupled to the swirl flow by the term $r^{-4}\delta^{-1}\partial V^2/\partial z$. The physical interpretation of this coupling term rests on the balance (to lowest order) between the radial pressure gradient and $v_\theta^2/r + v_\theta/\mathrm{Ro}$. In other words, a vertical gradient of the angular momentum implies a vertical pressure gradient that drives a meridional flow.

To study the interaction between the swirl flow and the meridional flow, we follow the approach taken by Lord Kelvin,[1] assuming a small perturbation V_1 of the basic vortex with absolute angular momentum V_0,

$$V = V_0 + V_1, \tag{13}$$

where $V_1 \ll V_0$ so that the conditions for linearization hold. In addition, the meridional flow satisfies $\Phi = \Phi_1 \ll V_0$, $\psi = \psi_1 \ll V_0$.

Substitution of Eq. (13) into Eqs. (8)–(10) yields to lowest order an equation for V_0,

$$\mathrm{N}\frac{\partial V_0}{\partial t} = \frac{1}{\mathrm{Re}} \left(r \frac{\partial}{\partial r} \frac{1}{r} \frac{\partial V_0}{\partial r} \right) + \frac{1}{\mathrm{Re}\,\delta^2} \frac{\partial^2 V_0}{\partial z^2}, \tag{14}$$

and hence, the basic state is only modified by diffusion. In addition, we obtain a set of equations for V_1, Φ_1, and ψ_1,

$$\mathrm{N}\frac{\partial V_1}{\partial t} + \frac{1}{r}[V_0, \psi_1] = \frac{1}{\mathrm{Re}} \left(r \frac{\partial}{\partial r} \frac{1}{r} \frac{\partial V_1}{\partial r} \right) + \frac{1}{\mathrm{Re}\,\delta^2} \frac{\partial^2 V_1}{\partial z^2}, \tag{15}$$

$$\mathrm{N}\frac{\partial \Phi_1}{\partial t} = \frac{2}{\delta r^4} \left(V_0 \frac{\partial V_1}{\partial z} + V_1 \frac{\partial V_0}{\partial z} \right) + \frac{1}{\mathrm{Re}} \left(\frac{\partial^2 \Phi_1}{\partial r^2} + \frac{3}{r} \frac{\partial \Phi_1}{\partial r} \right) + \frac{1}{\mathrm{Re}\,\delta^2} \frac{\partial^2 \Phi_1}{\partial z^2}, \tag{16}$$

$$\Phi_1 = \frac{1}{r^2} \tilde{\Delta} \psi_1, \tag{17}$$

where second order quantities have been neglected.

IV. INVISCID LINEAR THEORY

In this section, we study the inviscid limit $(\mathrm{Re} \to \infty)$ of Eqs. (14)–(17). If V_0 is z-independent, then $V_0 = V_0(r)$, and the combination of Eqs. (15)–(17) results in the following equation for ψ_1:

$$\frac{\partial^2}{\partial t^2} \tilde{\Delta} \psi_1 = -\frac{\eta(r)}{\delta} \frac{\partial^2 \psi_1}{\partial z^2}, \tag{18}$$

with

$$\eta(r) = \frac{1}{\mathrm{N}^2 r^3} \frac{\mathrm{d} V_0^2}{\mathrm{d} r}, \tag{19}$$

where η denotes the extended Rayleigh discriminant[12] normalized to 1 for $r = 0$.

Assume now a time-periodic perturbation $\psi_1 = \tilde{\psi}(r, z) e^{i\xi t}$, with ξ the frequency of the oscillation. Substitution of this form into the previous equation yields

$$\xi^2 \tilde{\Delta} \tilde{\psi} = \frac{\eta(r)}{\delta} \frac{\partial^2 \tilde{\psi}}{\partial z^2}. \tag{20}$$

Assuming a separable solution $\tilde{\psi}(r, t) = R(r) Z(z)$ leads to equations for R and Z,

$$\frac{1}{Z}\frac{d^2Z}{dz^2} = -\lambda^2, \tag{21}$$

$$r\frac{d}{dr}\left(\frac{1}{r}\frac{dR}{dr}\right) - \frac{\lambda^2}{\delta^2}R = -\frac{\lambda^2}{\delta^2}\left(\frac{\eta(r)}{\xi^2}\right)R, \tag{22}$$

where λ is the separation constant.

At the bottom ($z=0$) and at the rigid free surface ($z=1$), an impermeability condition is imposed ($\tilde{\psi}=0$). Together with these boundary conditions, Eq. (21) constitutes an eigenvalue problem for the eigenvalue λ, and the quantized solution is of the form

$$Z(z) = C_2 \sin(\lambda_n z), \tag{23}$$

where the vertical wave number is $\lambda_n=\pi(n+1)$, and the integer $n=0,1,2,\ldots$ is the vertical mode number.

Equation (22) is rewritten as

$$r\frac{d}{dr}\left(\frac{1}{r}\frac{dR}{dr}\right) - k_n^2 R = -k_n^2\frac{\eta(r)}{\xi_n^2}R, \tag{24}$$

where $k_n^2=\lambda_n^2/\delta^2$. Solutions to Eq. (24) are required to satisfy the following boundary conditions:

$$R(r=0) = R(r=\mathrm{R_c}\leq\infty) = 0. \tag{25}$$

With these homogeneous boundary conditions, Eq. (24) constitutes a Hermitian eigenvalue problem of Sturm–Liouville type for the eigenvalue ξ_n provided that $\eta(r)>0$ for $0<r<\mathrm{R_c}$, i.e., if the vortex is stable to centrifugal instability. This implies that all eigenvalues $\xi_{m,n}$ are discrete and real valued.

A. The role of horizontal confinement in the frequency range

The extended Rayleigh discriminant η can be rewritten as

$$\eta(r) = \frac{1}{(\mathrm{Ro}+1)^2}\left(1+\mathrm{Ro}\frac{2v_{\theta,0}}{r}\right)(1+\mathrm{Ro}\,\omega_{z,0}), \tag{26}$$

with $v_{\theta,0}=v_{\theta,0}(r)$ the azimuthal velocity of basic vortex, and $\omega_{z,0}=\omega_{z,0}(r)=(1/r)[d(rv_{\theta,0})/dr]$ the vorticity.

For vortices with $\omega_{z,0}$ monotonically decreasing in r, such as the Rankine vortex and the Lamb–Oseen vortex, $\omega_{z,0}=1+\mathcal{O}(r^2)$ and $v_{\theta,0}=r/2+\mathcal{O}(r^3)$ as $r\downarrow 0$, and $\omega_{z,0}\to 0$ and $v_{\theta,0}\to 0$ for $r\to\infty$ yielding

$$\eta(r) \to \begin{cases} 1, & r\downarrow 0 \\ \dfrac{1}{(\mathrm{Ro}+1)^2}, & r\to\infty. \end{cases} \tag{27}$$

The upper bound for the spectrum of $\xi_{m,n}$ can be determined by multiplying Eq. (24) by R/r and integrating over $0<r<\mathrm{R_c}$. Then, through integration by parts and using the boundary conditions, we obtain

$$0 \leq \xi_{m,n}^2 \leq \begin{cases} 1, & 0\leq \mathrm{Ro}<\infty \\ (\mathrm{Ro}+1)^{-2}, & -1<\mathrm{Ro}<0, \end{cases} \tag{28}$$

where we have assumed that $\eta(r)$ monotonically decreases (increases) from $\eta(0)=1$ to $\eta(\infty)=(\mathrm{Ro}+1)^{-2}$ for $0\leq\mathrm{Ro}<\infty$ ($-1<\mathrm{Ro}<0$). Note that for anticyclonic vortices, our study is restricted to $-1<\mathrm{Ro}<0$ since the vortices are prone to centrifugal instability and Eq. (24) is no longer an eigenvalue problem of the Sturm–Liouville type for $\mathrm{Ro}<-1$.

To clarify the meaning of the upper bounds for the frequency range, it is convenient to define the dimensional frequency $\xi_{m,n}^*=|\hat{\omega}_0+2\Omega|\xi_{m,n}$. Then, $\xi_{m,n}^2=1$ is equivalent to $\xi_{m,n}^{*2}=(\hat{\omega}_0+2\Omega)^2$ in dimensional units, while $\xi_{m,n}^2=(\mathrm{Ro}+1)^{-2}$ is equivalent to $\xi_{m,n}^{*2}=(2\Omega)^2$ in dimensional units.

If $\mathrm{R_c}=\infty$, it is useful to write Eq. (24) in normal form by taking $R=\sqrt{r}F$,

$$\frac{d^2F}{dr^2} + \left[k_n^2\left\{\frac{\eta(r)}{\xi_{m,n}^2}-1\right\} - \frac{3}{4r^2}\right]F = 0. \tag{29}$$

To satisfy the boundary condition for $r\to\infty$, the term $\eta(r)/\xi_{m,n}^2$ in Eq. (29) must satisfy

$$\frac{\eta(\infty)}{\xi_{m,n}^2} < 1, \tag{30}$$

which, using Eq. (27), implies that

$$\xi_{m,n}^2 > (\mathrm{Ro}+1)^{-2}. \tag{31}$$

Combining this with Eq. (28), we conclude that for $\mathrm{R_c}=\infty$,

$$(\mathrm{Ro}+1)^{-2} < \xi_{m,n}^2 \leq 1 \quad \text{for} \quad 0\leq\mathrm{Ro}<\infty, \tag{32}$$

and no modes are possible for $-1<\mathrm{Ro}<0$.

Condition (32) implies that in an infinite domain no modes with frequencies smaller than the rotation rate of the system [$\xi_{m,n}^2<(\mathrm{Ro}+1)^{-2}$] exist, while these frequencies are sustained within a domain bounded in the r-direction ($\mathrm{R_c}<\infty$).

For Kelvin waves in a nonconfined ($\mathrm{R_c}=\infty$) Lamb–Oseen vortex with background rotation, Eq. (22) was studied recently by Le Dizès[13] using a WKBJ approach based on the vertical wave number being large. Le Dizès found nontrivial solutions to Eq. (22) that satisfy the homogeneous Dirichlet conditions $R(r)=0$ at $r=0$ and $r=\mathrm{R_c}=\infty$ for $(\mathrm{Ro}+1)^{-2}<\xi_{m,n}^2<1$ (that is, the absolute value of the dimensional frequency is between 2Ω and $2\Omega+\hat{\omega}_0$). However, no solutions were found for $0<\xi_{m,n}^2<(\mathrm{Ro}+1)^{-2}$ in agreement with condition (32).

The physical difference between the two different boundary conditions can be explained as follows. When $\mathrm{R_c}=\infty$, the wave must be outgoing or exponentially small at infinity; this condition is known as a radiative boundary condition. However, reflections are also allowed at the boundary when $\mathrm{R_c}<\infty$.

B. The Rankine vortex

To solve the eigenvalue problem equation (24) analytically, we focus on a relatively simple vortex profile, namely, the Rankine vortex confined to a rotating cylinder. The structure of the Rankine vortex consists of a core of uniform vorticity and an irrotational exterior, and is given, in terms of the absolute angular momentum, by

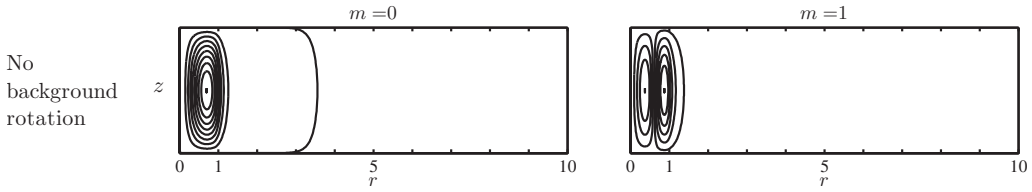

FIG. 2. Streamlines of the inertial waves sustained by a Rankine vortex without background rotation. Isolines of $\tilde{\psi}$ for Ro=∞, R_c=10, δ=0.5, and mode numbers n=0 and m=0,1.

$$V_0(r) = \begin{cases} \dfrac{r^2}{2} + \dfrac{r^2}{2\,\mathrm{Ro}}, & 0 \le r < 1 \\ \dfrac{1}{2} + \dfrac{r^2}{2\,\mathrm{Ro}}, & 1 \le r \le R_c. \end{cases} \tag{33}$$

For this profile the solution to Eq. (24) is presented in detail in Appendix A.

An example of the streamlines in the r,z-plane for a Rankine vortex without background rotation is shown in Fig. 2 for δ=0.5 and mode numbers n=0 and m=0,1. As can be seen, the secondary flow is composed of recirculation cells, where $n+1$ gives the number of cells in the vertical direction, and $m+1$ gives the number of cells in the radial direction. For Ro=∞, $\tilde{\psi}$ outside the vortex core ($r>1$) is given in terms of evanescent, modified Bessel functions, the meridional flow is irrotational (Φ=0), and V_1=0 as found by Lord Kelvin.[1]

1. Cyclonic vortices

For cyclonic vortices ($0<\mathrm{Ro}<\infty$), the maximum frequency allowed is such that $\xi^2_{m,n}=1$, as shown in Eq. (28). Thus, the streamfunction $\tilde{\psi}$ inside the vortex core ($r<1$) is given in terms of J_1, the Bessel function of the first kind and order one [see Eq. (A5)].

On the other hand, outside the vortex core ($r>1$) there are three qualitatively different regimes that depend on the value of the frequency $\xi_{m,n}$:

(a) *Regime CI*: $1>\xi^2_{m,n}>(\mathrm{Ro}+1)^{-2}$ and $\xi^2_{m,n}>k_n^2/(\mathrm{N}^2\,\mathrm{Ro})$. In this regime, the streamfunction $\tilde{\psi}$ in the outer region is given in terms of modified Bessel functions of order $\gamma\in\mathbb{R}$ [see Eq. (A8)]. Hence, the streamfunction has an exponentially decaying tail outside the vortex core as for Ro=∞. See, for example, the upper panels in Fig. 3.

(b) *Regime CII*: $1>\xi^2_{m,n}>(\mathrm{Ro}+1)^{-2}$ and $\xi^2_{m,n}<k_n^2/(\mathrm{N}^2\,\mathrm{Ro})$. In this regime, the streamfunction $\tilde{\psi}$ in the outer region is given in terms of modified Bessel functions of imaginary order ($\gamma\in\mathbb{I}$). In this case, the streamfunction can have an oscillatory behavior in r outside the vortex core, but still an exponentially decaying tail exists next to the outer wall. See, for example, the middle panels in Fig. 3.

(c) *Regime CIII*: $(\mathrm{Ro}+1)^{-2}>\xi^2_{m,n}>0$. In this case, the streamfunction $\tilde{\psi}$ is given in terms of Bessel functions [see Eq. (A17)], which have an oscillatory behavior in r that extends radially across the whole cylinder, as shown in the bottom panels of Fig. 3. In this regime, $\tilde{\psi}$ is similar to the streamfunction obtained for inertial

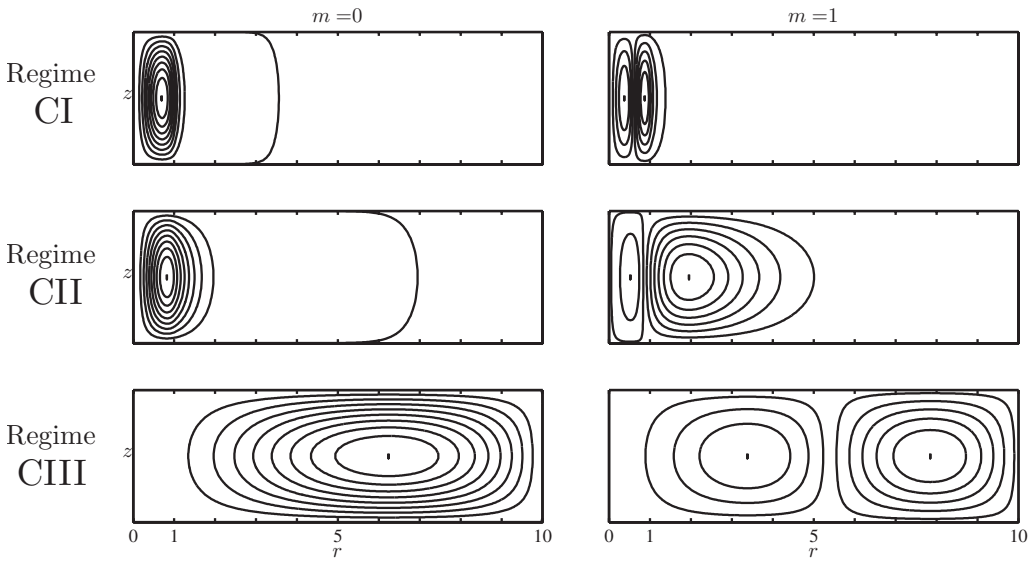

FIG. 3. Three regimes for the streamlines of the inertial modes sustained by a Rankine vortex with background rotation. Isolines of $\tilde{\psi}$ for R_c=10, δ=0.5, and mode numbers n=0 and m=0,1 for different values of Ro. Regime CI (top): Ro=100, $(\mathrm{Ro}+1)^{-1}\approx0.01$, and $k_n^2/(\mathrm{N}^2\,\mathrm{Ro})\approx0.39$, while $\xi_{0,0}\approx0.71$ and $\xi_{0,1}\approx0.55$. Regime CII (middle): Ro=0.25, $(\mathrm{Ro}+1)^{-1}=0.8$, and $k_n^2/(\mathrm{N}^2\,\mathrm{Ro})\approx6.32$, while $\xi_{0,0}\approx0.87$ and $\xi_{0,1}\approx0.81$. Regime CIII (bottom): Ro=0.02, $(\mathrm{Ro}+1)^{-1}\approx0.980$, and $k_n^2/(\mathrm{N}^2\,\mathrm{Ro})\approx0.759$, while $\xi_{0,0}\approx0.979$ and $\xi_{0,1}\approx0.975$.

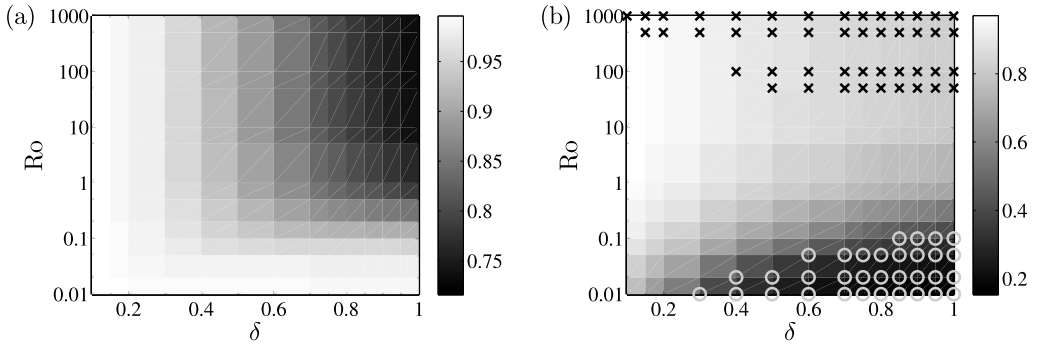

FIG. 4. Graphical representation of the frequency and the wave number of mode $(m,n)=(0,0)$ as a function of Ro and δ. The grayscale denotes (a) the absolute value of the frequency $|\xi_{0,0}|$ and (b) the normalized wave number $\bar{\alpha}_{0,0}$ for $R_c=10$ as a function of Ro and δ. The crosses in (b) mark the solutions corresponding to regime CI, while the circles mark the solutions corresponding to regime CIII.

oscillations inside a rotating cylinder without a vortex in the center (see Ref. 3). Note that this regime does not exist in the case $R_c=\infty$. In fact, we show in Appendix A that in this regime, the solution to Eq. (24) for a Rankine vortex cannot satisfy the boundary condition $\psi\to 0$ as $r\to\infty$.

As has been seen in Figs. 2 and 3, the secondary flow is composed of recirculation cells. These cells redistribute the angular momentum V, changing its vertical distribution. Subsequently, the recirculation cells reverse their direction due to the change in the vertical gradient of V, and this interaction repeats itself.

In fact, the evolution of the absolute angular momentum of the swirl flow, following Eq. (15), is given by

$$V(r,z,t)=V_0(r)+\tilde{V}_1(r)\cos(\lambda_n z)e^{i(\xi_{m,n}t+\pi/2)}, \tag{34}$$

where

$$\tilde{V}_1(r)=\epsilon\frac{\lambda_n}{\xi_{m,n}}\begin{cases} R(r), & 0\le r<1 \\ \dfrac{1}{\mathrm{Ro}+1}R(r), & 1\le r\le R_c, \end{cases} \tag{35}$$

with $\epsilon\ll\xi_{m,n}/\lambda_n$, and $R(r)$ is the r-dependence of the streamfunction $\tilde{\psi}$. Note that the frequency of the oscillation in V is equal to the frequency of the oscillations in the secondary motion but out of phase by a quarter period.

Furthermore, $\tilde{V}_1$ has a discontinuity at $r=1$ for $\mathrm{Ro}\neq 0$. This discontinuity is consistent with the fact that $\tilde{V}_1=0$ outside the vortex core for $\mathrm{Ro}=\infty$,[1] whereas for $\mathrm{Ro}=0$, the discontinuity disappears, and the solution for a rotating cylinder without a vortex is retrieved (see Ref. 3). Independent of the frequency $\xi_{m,n}$, if $\mathrm{Ro}\neq 0$, then $V_1\neq 0$ outside the vortex core, and the oscillations of the azimuthal motion are no longer confined to the inside of the vortex core. However, the amplitude of V_1 outside the vortex core can be negligible for large Ro values.

We have shown that the recirculation cells can differ qualitatively depending on the value of the frequency $\xi_{m,n}$. Furthermore, the values of $\xi_{m,n}$ depend on the problem parameters: Ro, δ, and R_c. Figure 4(a) shows the absolute value of the frequency for mode $(m,n)=(0,0)$, i.e. $|\xi_{0,0}|$, for $R_c=10$ as a function of Ro and δ. As can be seen, the frequency of the zero mode tends to unity as $\delta\to 0$ and $\mathrm{Ro}\to 0$, while the lowest frequencies are reached for slow rotation (large Ro values) and large aspect ratio δ when keeping R_c fixed.

Figure 4(b) shows the normalized wave number inside the vortex core $\bar{\alpha}_{0,0}=\alpha_{0,0}/j_{1,0}$ [with $j_{1,0}$ the first zero of J_1 and $\alpha_{0,0}$ the wave number inside the vortex core, as defined in Eq. (A4)] for $R_c=10$ as a function of Ro and δ. As can be seen, the wave number is smaller for fast rotation rates (small Ro values) and large aspect ratio δ. It is in this region of the parameter space that the zeroth mode occupies the whole cylinder, as shown by the circles that denote regime CIII. Furthermore, the wave number is larger for slow rotation rates (large Ro) and small aspect ratio. It is in this region when the recirculation cell is smaller in the radial direction. Surprisingly, this behavior does not correspond to the regime CI denoted by the crosses. However, it is clear that a smaller aspect ratio δ tends to reduce the radial extent of the oscillations, while strong rotation tends to increase it.

As the mode number m increases, the frequency $\xi_{m,n}$ decreases for fixed mode number n. Hence, the boundary between the different regimes depends on the mode number. In other words, even if, for example, mode $(m,n)=(0,0)$ corresponds to regime CII there can be a mode (m,n) with $m>0$ in regime CIII for the same values of the problem parameters.

After pointing out, in Sec. IV A, the differences in attainable frequencies of the inertial oscillations in finite and infinite domains, we have restricted our study to the case $R_c=10$. In Fig. 5(a), we present the value of the frequency $\xi_{0,0}$ for fixed $\delta=1$ as a function of Ro and R_c, while in Fig. 5(b), we present the value of $\xi_{0,0}$ for fixed $\mathrm{Ro}=1$ as a function of δ and R_c. As can be clearly seen, the frequency does not depend strongly on R_c for large values of this parameter.

2. Anticyclonic vortices

It was shown in Eq. (28) that for anticyclones $(-1<\mathrm{Ro}<0)$ the frequency is such that $\xi_{m,n}^2<(\mathrm{Ro}+1)^{-2}$. Hence, outside the vortex core, the solution to Eq. (24) is given in terms of Bessel functions [see Eq. (A17)] and the recirculation cells extend to the outer wall.

On the other hand, there are two qualitatively different regimes inside the vortex core:

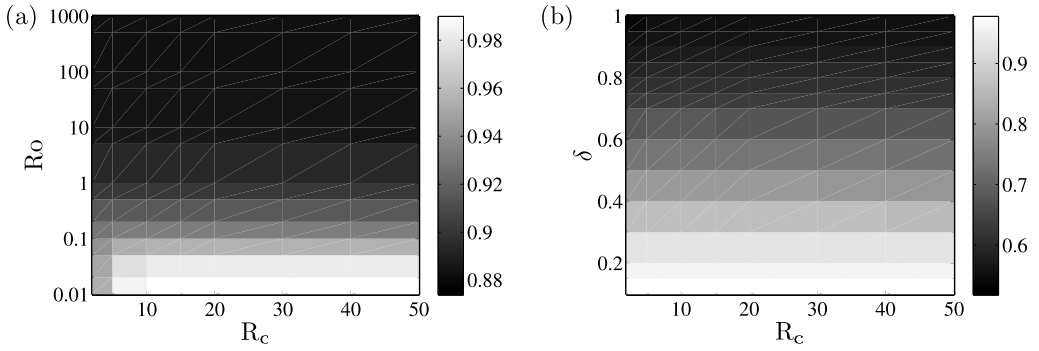

FIG. 5. Graphical representation of the frequency of mode $(m,n)=(0,0)$ for a Rankine vortex as a function of Ro, δ, and R_c. (a) Grayscale denotes values of the frequency $\xi_{0,0}$ for fixed $\delta=1$ as a function of Ro and R_c. (b) Values of the frequency $\xi_{0,0}$ for fixed Ro=1 as a function of δ and R_c.

(a) *Regime AI*: $(\mathrm{Ro}+1)^{-2}>\xi_{m,n}^2>1$. In this regime, the solution to Eq. (24) inside the vortex core is given in terms of $I_1(\alpha r)$, the modified Bessel function of the first kind and order one [see Eq. (A5)]. Hence, the streamfunction $\tilde{\psi}$ cannot have an oscillatory behavior in r inside the vortex core. An example of such a flow is presented in Fig. 6(a), where the streamlines of the secondary flow for $(m,n)=(0,0)$, Ro=−0.5, $\delta=0.5$, and $R_c=10$ are plotted.

(b) *Regime AII*: $1>\xi_{m,n}^2>0$. In this regime, the solution to Eq. (24) inside the vortex core is given in terms of $J_1(\alpha r)$, the Bessel function of the first kind and order one [see Eq. (A5)]. Hence, the recirculation can have an oscillatory behavior in r across the whole cylinder. This can be seen in Fig. 6(b), where the streamlines for $(m,n)=(0,0)$, Ro=−0.01, $\delta=0.5$, and $R_c=10$ are plotted.

C. The Lamb–Oseen vortex

The Rankine vortex is a crude approximation for a real vortex, and it is by nature an inviscid model. To later consider the effects of viscosity, we study the waves sustained by a the Lamb–Oseen vortex, which is a good approximation to some real vortices (see, e.g., Ref. 12). In this section, we consider a time-independent Lamb–Oseen vortex with a velocity profile given by

$$v_{\theta,0}(r)=\frac{1}{2r}[1-\exp(-r^2)]. \tag{36}$$

This vortex is characterized by a strong stability. For example, although it can be unstable with respect to centrifugal instability, this is only the case for strong anticyclonic vortices with Ro<−1 (Ref. 12) as for the Rankine vortex. Furthermore, it is stable to shear instability,[8] and as long as there is no elliptical perturbation also to elliptical instability. This stability backs our assumption of azimuthal symmetry.

The absolute angular momentum for the Lamb–Oseen vortex is given by

$$V_0(r)=\frac{1}{2}[1-\exp(-r^2)]+\frac{r^2}{2\,\mathrm{Ro}}. \tag{37}$$

For this profile, Eq. (24) cannot be solved analytically; hence, the eigenvalue problem is solved numerically with the finite element code COMSOL—using the one-dimensional general form partial differential equations module with the UMFPACK solver and 120 elements (see Ref. 14).

The dynamics of the axisymmetric inertial oscillations sustained by a Rankine vortex is similar for a Lamb–Oseen vortex in the nonrotating case,[5] as in the case with background rotation. However, some differences in the characteristics of such oscillations exist.

Figure 7(a) presents the ratio of $\xi_{0,0}$ for Lamb–Oseen vortex to $\xi_{0,0}$ for a Rankine vortex as a function of Ro and δ for $R_c=10$. As can be seen, this ratio tends to unity as the rotation rate increases; already for Ro<1, the frequency ratio does not exceed 10%. For large Ro values and large δ-values—in regime CI—the difference in frequencies is most important. In contrast, specially in regime CIII, the frequency ratio is close to unity. This can be easily explained, since for small Ro values the vortex motion is very weak compared with the background rotation.

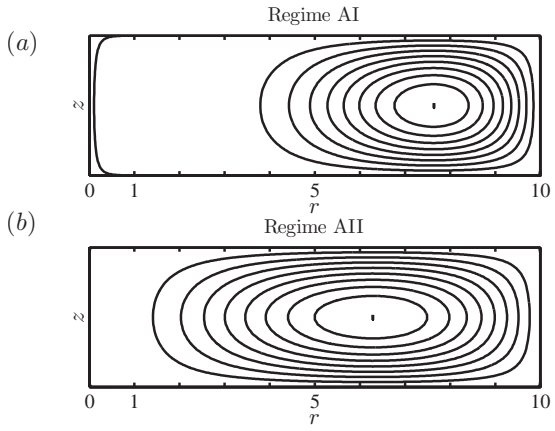

FIG. 6. (a) Isolines of $\tilde{\psi}$ for Ro=−0.5, $R_c=10$, $\delta=0.5$, and $(m,n)=(0,0)$. In this case $\xi_{0,0}\approx 1.983>1$ corresponding to regime AI. (b) Isolines of $\tilde{\psi}$ for Ro=−0.001, $R_c=10$, $\delta=0.5$, and $(m,n)=(0,0)$. In this case $\xi_{0,0}\approx 0.991<1$ corresponding to regime AII.

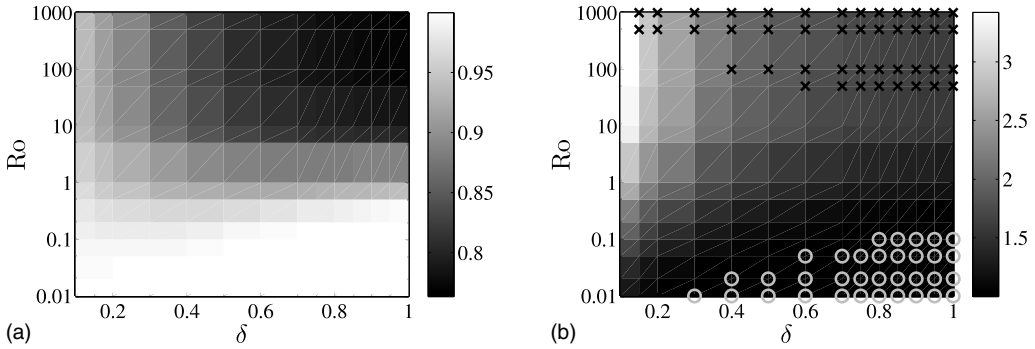

FIG. 7. Graphical representation of the characteristics of mode $(m,n)=(0,0)$ for the Lamb–Oseen vortex compared with the characteristics of mode $(m,n)=(0,0)$ for the Rankine vortex. The grayscale denotes (a) the ratio of $|\xi_{0,0}|$ for the Lamb–Oseen vortex and $|\xi_{0,0}|$ for the Rankine vortex and (b) the ratio of $\bar{\alpha}_{0,0}$ for the Lamb–Oseen vortex and for $\bar{\alpha}_{0,0}$ for the Rankine vortex for $R_c=10$ as a function of Ro and δ. The crosses in (b) mark the points that correspond to regime CI, while the circles mark the points that correspond to regime CI.

Figure 7(b) shows the ratio of $\alpha_{0,0}$ for a Lamb–Oseen vortex to $\alpha_{0,0}$ for a Rankine vortex. As can be seen, for small Ro values this ratio tends to unity suggesting that the radial wave number does not depend on the velocity profile. However, when rotation is decreased, the wave number $\alpha_{0,0}$ for the Lamb–Oseen vortex becomes up to three times larger than the wave number for the Rankine vortex for small aspect ratio δ. This can be explained as follows. For the Rankine vortex, waves with frequencies close to unity can be sustained inside the whole vortex core since the frequency is smaller than $2\Omega+\hat{\omega}$ for $0<r<1$. However, for the Lamb–Oseen vortex, the waves with frequencies approaching unity can only be sustained in a smaller domain.

In Fig. 7(b) the crosses denote the parameter for which mode $(m,n)=(0,0)$ is in regime CI, while the circles denote the parameters for which mode $(m,n)=(0,0)$ is in regime CIII. As can be seen by comparison to Fig. 4(b), the boundary between the different regimes agrees well for both vortex profiles. Furthermore, the characteristics of the three different regimes for cyclonic Rankine vortices are similar for a Lamb–Oseen vortex.

V. THE EFFECTS OF VISCOSITY

A. In a cylinder with stress-free boundaries

When considering a time-independent Lamb–Oseen vortex, as in Sec. IV C, the effect of viscosity on axisymmetric inertial oscillations is rather trivial. As found by Fabre *et al.*[5] for the case of no background rotation, viscosity only damps the oscillations. By assuming $k_n \ll \alpha_m$, we show in Appendix B that the slowest decay rate given by

$$T^{-1} = k_n^2/(\mathrm{N\ Re}). \tag{38}$$

However, viscosity also affects the main azimuthal motion. For the Lamb–Oseen vortex, the time-dependent azimuthal-velocity profile is given by the self-similar solution to Eq. (14),

$$v_{\theta,0}(r,t) = \frac{1}{2r}\left[1 - \exp\left(-\frac{r^2}{1+4t/(\mathrm{N\ Re})}\right)\right], \tag{39}$$

when taking Eq. (37) as the initial condition. The corresponding vertical vorticity component is given by

$$\omega_{z,0}(r,t) = \frac{1}{1+4t/(\mathrm{N\ Re})}\exp\left(-\frac{r^2}{1+4t/(\mathrm{N\ Re})}\right). \tag{40}$$

As can be seen from Eqs. (39) and (40), both the radius and the peak vorticity of the vortex change over time. Hence, it is possible to define a time-dependent Rossby number

$$\mathrm{Ro}_T(t) = \frac{\mathrm{Ro}}{1+4t/(\mathrm{N\ Re})} \tag{41}$$

and a time dependent aspect ratio

$$\delta_T(t) = \frac{\delta}{\sqrt{1+4t/(\mathrm{N\ Re})}}, \tag{42}$$

both decreasing in time. Combining Eqs. (41) and (42) yields

$$\delta_T = K\sqrt{\mathrm{Ro}_T}, \tag{43}$$

where K is constant.

As it was seen in Sec. IV B, if both Ro and δ decrease, then the frequency tends to the maximum frequency allowed, which is now given by

$$\xi_{\max}(t) = \frac{1+\mathrm{Ro}_T(t)}{1+\mathrm{Ro}} \tag{44}$$

for the time-dependent Lamb–Oseen vortex.

To understand how the wave number changes in time, we consider that $\xi \gg 4/(\mathrm{N\ Re})$. In this case, we can assume that the vortex is frozen at every instant since the time scales for the oscillations and for the vortex decay can be separated. We also assume that R_c remains large as to not affect the value of the frequency and the wave number.

Figure 8 shows the absolute value of the wave number $|\alpha_{0,0}|$ for a Lamb–Oseen vortex as a function of Ro and δ for $R_c=20$. In addition, this figure also shows curves given by Eq. (43) for different values of K. The evolution of the Lamb–Oseen vortex follows these curves from right to left. As can be seen, for large Ro values, the wave number $|\alpha_{0,0}|$ increases in time. However, when the initial values for Ro and δ are close to the boundary between the regimes CII and CIII, then the wave number remains almost constant. Hence, there is a value for K for which Eq. (43) gives a boundary between the two regimes.

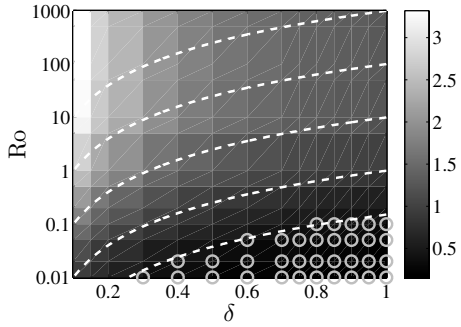

FIG. 8. Evolution of the frequency of mode $(m,n)=(0,0)$ sustained by a time-dependent Lamb–Oseen vortex. The grayscale denotes the normalized wave number $\bar{\alpha}_{0,0}$ for the oscillations sustained by a Lamb–Oseen vortex with $R_c=20$ as a function of Ro and δ. The circles mark the points where $|\xi_{0,0}|<(\mathrm{Ro}+1)^{-1}$, while the dashed lines are given by Eq. (43) for different values of K.

B. The effects of a no-slip bottom

We performed numerical simulations where Eqs. (3)–(5) inside a cylinder with a no-slip bottom were solved. The initial condition was taken to be a Lamb–Oseen vortex with no vertical dependence and no perturbation [Eq. (37)]. Although this initial condition does not satisfy the no-slip boundary condition at the bottom, the initial flow is adjusted instantaneously by the numerical code to satisfy the boundary condition. Several simulations were performed with different initial z-dependence to test if these profiles affected the results. We found that there were no significant differences when a small boundary layer was added to the initial vertical profile.

The simulations were performed using the finite element code COMSOL with the two-dimensional-axisymmetric incompressible Navier–Stokes module, approximately 140 000 degrees of freedom, and the PARDISO solver (see Ref. 14). Both the time and spatial resolution were evaluated by performing several numerical simulations with different resolutions, and verifying that the results converged to the same solution.

1. No background rotation

First, we analyze a vortex without background rotation. In this case, when δ and Re are small, the main flow has a Poiseuille-like vertical profile and is damped at a rate $\pi^2/(4\,\mathrm{Re}\,\delta^2\mathrm{N})$ since the evolution is dominated by viscosity.[15] For these values of δ and Re, no inertial oscillations are sustained inside the vortex.

However, for larger values of δ and Re, the vertical profile of the main flow differs from Poiseuille-like. Figure 9 shows the vertical profile of the azimuthal velocity v_θ and streamlines in the r,z-plane at $t=5$ for a simulation with $\mathrm{Re}=2500$, $\delta=0.5$, $\mathrm{Ro}=\infty$, and $R_c=12$. From the vertical profile of v_θ, we can see that a boundary layer forms close to the bottom, and that on top of it, the flow is more uniform in the vertical direction. The streamlines in the r,z-plane show a large secondary motion that occupies the whole depth of the fluid. The recirculation cell shown in Fig. 9 is driven by the boundary layer unlike the recirculation cells shown in the previous sections, which are associated with the inertial oscillations.

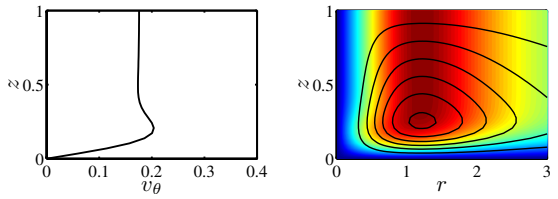

FIG. 9. (Color online) Lamb–Oseen vortex inside a cylinder with a no-slip bottom and no background rotation. Vertical profile of v_θ at $r=0.5$ (left), contours of the secondary flow, and azimuthal velocity (color/grayscale) (right) at $t=5$ for a simulation with $\mathrm{Re}=2500$, $\delta=0.5$, $\mathrm{Ro}=\infty$, and $R_c=12$.

Figure 10 presents snapshots of the azimuthal velocity and the streamlines in the r,z-plane at three different times, and of the vertical profile of the pressure $p(z)$ in the vortex core $(r=0.01)$ at three different times for a simulation with $\mathrm{Ro}=\infty$, $\mathrm{Re}=2500$, $\delta=0.5$, and $R_c=12$. As can be seen, the vertical pressure gradient changes sign in time. This is due to the presence of inertial oscillations, which are superimposed to the secondary motion. The physical process driving these oscillations, as observed in Fig. 10, can be described as follows. Initially on the vortex axis, a negative vertical pressure gradient exists, which drives an upward motion in the vortex core, and hence, a meridional flow. This flow redistributes the azimuthal velocity. Consequently, the vertical gradient of the azimuthal velocity and the pressure are inverted. This new pressure gradient forces a downward motion in the center of the vortex and the appearance of a cell in the meridional flow with an opposite direction to the main secondary flow driven by the boundary layer. This process repeats itself, always with the oscillation in the pressure out of phase by a quarter period with respect to the oscillation in the meridional flow. It can also be seen in the pressure profiles that at the top of the boundary layer $(z\sim0.1)$ the pressure gradient is always negative, thus continuously driving the large recirculation cell.

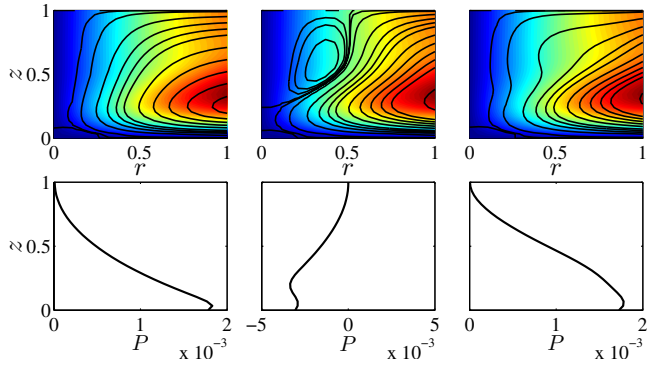

FIG. 10. (Color online) Evolution of a Lamb–Oseen vortex inside a cylinder with a no-slip bottom and no background rotation. Upper row: meridional circulation at three different times $(t=5,10,17.5)$ for $\mathrm{Ro}=\infty$, $\mathrm{Re}=2500$, and $\delta=0.5$. The color/grayscale coding denotes the azimuthal velocity and the black lines are streamlines of the secondary flow in the r,z-plane. Lower row: pressure profile at $r=0.01$ and three different times $(t=1,7.5,15)$ for the same simulations.

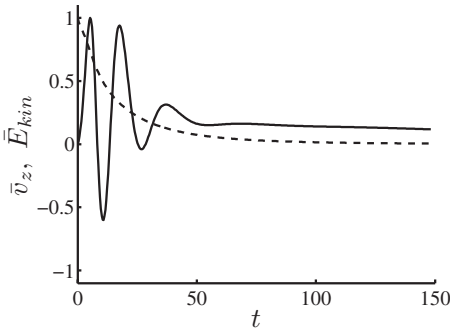

FIG. 11. Evolution of the normalized vertical velocity $\bar{v}_z=v_z/\max(v_z)$ in the core of the vortex $(r,z)=(0.01,0.8)$ (solid line) and evolution of the normalized kinetic energy of the azimuthal motion $\bar{E}_{\mathrm{kin}}=E_{\mathrm{kin}}/\max(E_{\mathrm{kin}})$ (dashed line) for a simulation with Re=2500, $\delta=0.5$, Ro=∞, and $\mathrm{R_c}=12$.

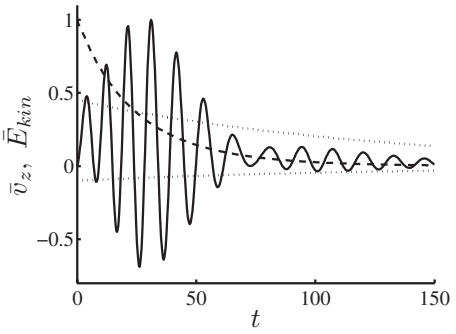

FIG. 13. Normalized vertical velocity $\bar{v}_z=v_z/\max(v_z)$ in the vortex core $(r,z)=(0.01,0.8)$ (solid lines) and normalized kinetic energy of the main azimuthal motion $\bar{E}_{\mathrm{kin}}=E_{\mathrm{kin}}/\max(E_{\mathrm{kin}})$ (dashed line) for a simulation Ro=1, Re=2500, $\delta=0.5$, and $\mathrm{R_c}=12$. The dotted lines represent the envelope curves with a decay rate given by Eq. (38).

The presence of a no-slip boundary condition at the bottom has two main effects on the primary motion: (1) the main flow is damped faster due to bottom friction and (2) the main flow is modified by the secondary flow driven by the boundary layer. However, since advection plays an important role for large values of Re and δ, there is no analytical expression for the damping rate of the vortex or for its deformation.

Figure 11 shows the evolution of the normalized vertical velocity $v_z/\max(v_z)$ in the core of the vortex at $(r,z)=(0.01,0.8)$ and the evolution of the kinetic energy of the main azimuthal flow for a simulation with Re=2500, $\delta=0.5$, and Ro=∞. As can be seen, the vertical velocity inside the vortex oscillates. These oscillations are damped, and their frequency decreases in time due to the damping of the vortex and the growth of the vortex radius. By comparison to the decay of the kinetic energy of the vortex, it can be seen that the characteristic decay time of the main flow is a good estimate for the lifetime of the oscillations.

The type of flow discussed in this section and shown in Fig. 9 is similar to the one described by Akkermans *et al.*,[16] who studied an electromagnetically generated dipolar vortex in a shallow layer. In that case $\mathrm{Re}\approx 3500$ and $201\leq \mathrm{Re}\,\delta^2\leq 727$. In such a flow, a boundary layer at the bottom and inertial oscillations in the vortex cores on top of the boundary layer were observed.

2. Strong background rotation

For the case of strong rotation, the main flow consists of an Ekman boundary layer at the bottom and a geostrophic interior. This can be seen in Fig. 12, where snapshots of the azimuthal velocity and the streamfunction in the r,z-plane at three different times are shown for a simulation with Ro=1, Re=2500, $\delta=0.5$, and $\mathrm{R_c}=12$.

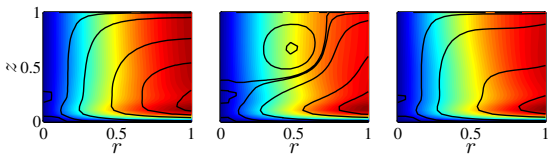

FIG. 12. (Color online) Evolution of a Lamb–Oseen vortex inside a cylinder with a no-slip bottom and background rotation. Upper row: meridional flow at three different times $(t=12.5,17.5,20)$ for Ro=1, Re=2500, $\delta=0.5$, and $\mathrm{R_c}=12$. The color/grayscale coding denotes the azimuthal velocity and the black lines are streamlines of the secondary flow in the r,z-plane.

As for the case of no background rotation, if viscous forces dominate, no inertial oscillations are sustained by the flow. For strong background rotation, this occurs when the thickness of the Ekman boundary layer

$$\delta_E=\mathrm{Ek}^{1/2}=\frac{1}{\delta}\left(\frac{2\ \mathrm{Ro}}{\mathrm{Re}}\right)^{1/2} \tag{45}$$

($\delta_E=\sqrt{\nu/\Omega}$ in dimensional units) is larger than the total layer depth $\delta_E>1$. Hence, we focus on flows with $\delta_E\ll 1$.

In Fig. 12, it can be observed, by comparison to Fig. 10, that the flow and the physical process driving the inertial oscillations are similar for flows with and without background rotation. However, in the rotating case (Ro=1), the recirculation cell associated with the inertial oscillations extends farther toward the exterior of the vortex, suggesting that the radial wavelength of the oscillations is larger.

Figure 13 displays the evolution of the normalized vertical velocity $v_z/\max(v_z)$ in the core of the vortex at $(r,z)=(0.01,0.8)$ and the kinetic energy of the azimuthal flow as a function of time for a simulation with Ro=1, Re=2500, $\delta=0.5$, and $\mathrm{R_c}=12$. As can be seen, the vertical velocity in the vortex core oscillates. Initially, the signal seems to be modulated, but this is due to the superposition of different modes with similar frequencies. In addition for Ro=1, the oscillation is persistent throughout the simulation for a much longer time than in the case of Ro=∞ (Fig. 11). As seen previously, for Ro=∞, no oscillations can be sustained once the vortex is damped. On the other hand, for Ro=1, the system still sustains oscillations even after the vortex has been damped. In this case, the decay rate of the oscillations is closer to the damping rate given by Eq. (38).

It could be argued that the inertial oscillations in the simulations discussed in this section arise because the flow must adjust itself since the initial condition has no vertical dependence. To exclude this possibility, we performed also simulations where the flow was forced for some time. For these simulations, $\boldsymbol{v}=0$ at $t=0$, and a forcing term

$$F = \frac{F_0}{2}[1 - \exp(-r^2)], \tag{46}$$

where F_0 is the magnitude of the forcing, was included on the right hand side of Eq. (8) for $0 < t < T_F$, where T_F is the forcing time. Inertial oscillations were also observed in these simulations, except when $T_F \gg 1$. Hence, we conclude that the inertial oscillations observed in previous numerical simulations are indeed a physical phenomenon.

The simulations discussed here were all performed under the assumption of axisymmetric flow, hence restricting the emergence of other modes, and other three-dimensional (3D) phenomena. To study this restriction, 3D simulations were performed for a few points in the parameter space. These simulations are computationally more expensive, thus it was not possible to achieve the same resolution as in the axisymmetric simulations. No qualitative differences were observed between the two types of simulations; however only some small quantitative differences, most likely caused by the lower spatial and temporal resolution of the 3D simulations, were found.

VI. CONCLUSIONS

We have studied the evolution of axisymmetric inertial oscillations in a confined monopolar vortex with background rotation and their effects on the evolution of the vortex itself. First, we presented an analytical result for the inviscid inertial oscillations sustained by the Rankine vortex inside a rotating cylinder. Later, numerical results for the inviscid waves sustained by a Lamb–Oseen vortex were analyzed. Finally, we studied the effects of viscosity and of a no-slip bottom on the evolution of the oscillations. In this way, a situation similar to the one found in laboratory experiments was reached, while discussing different properties of the oscillations at every step.

From the linear inviscid theory, we showed that the frequency range of the inertial oscillations in cyclonic vortices is such that $0 < \xi^{*2}_{m,n} < (2\Omega + \hat{\omega})^2$ (in dimensional units), where Ω is the rotation rate of the system and $\hat{\omega}$ is the peak vorticity of the vortex. However, horizontal confinement is necessary for modes with the absolute value of their frequency $|\xi^*_{m,n}| < 2\Omega$.

In the case with background rotation, the oscillations in the azimuthal flow can extend outside the vortex, as opposed to the case without background rotation. Furthermore, we found three qualitatively different regimes for the modes sustained by cyclonic vortices. It is in the regime where $\tilde{\xi}^2_{m,n} < (2\Omega)^2$, which only exists for horizontally confined vortices, that the streamfunction in the r,z-plane has an oscillatory behavior in r across the whole cylinder. This behavior is characteristic for strong rotation and large aspect ratio.

The effects of viscosity are twofold. On one hand, it acts directly on the oscillations by damping them. On the other hand, it acts on the main vortex by damping it and changing its radius. In this way, the characteristics of the waves sustained by the vortex change. For the cases when stress-free boundaries are considered, the basic vortex is a Lamb–Oseen vortex, and the decay rate of the vortex is much slower than the frequency of the oscillations, then the inviscid theory can be used to obtain the results at any given time.

On the other hand, when a no-slip bottom is considered, there is a boundary layer at the bottom which drives a meridional flow, and bottom friction damps the vortex. The meridional flow affects the evolution of the basic vortex, for which there is no analytical expression. In this case, the inertial oscillations are superimposed to the main meridional flow driven by the boundary layer. For the case of no background rotation, the oscillations cannot persist as the vortex is damped and their lifetime is hence dictated by the lifetime of the vortex. However, when background rotation is present the waves persist even if the vortex is damped since the system can still sustain oscillations.

This study was restricted to axisymmetric dynamics. In this case, confinement plays a crucial role in the frequency range of the oscillations sustained by a vortex subjected to background rotation. It is to be expected that confinement will also play an important role in nonaxisymmetric dynamics, and possibly in the stability of some vortices. This role is still to be determined.

ACKNOWLEDGMENTS

M.D.M. gratefully acknowledges the financial support from CONACYT (Mexico).

APPENDIX A: RADIAL DEPENDENCE OF THE INERTIAL OSCILLATIONS IN A RANKINE VORTEX

This appendix presents the detailed solution of Eq. (24),

$$r\frac{\mathrm{d}}{\mathrm{d}r}\left(\frac{1}{r}\frac{\mathrm{d}R}{\mathrm{d}r}\right) - k_n^2 R = -k_n^2 \frac{\eta(r)}{\xi^2} R, \tag{A1}$$

for the Rankine vortex given in Eq. (33).

1. Interior ($r<1$)

In the interior of the vortex the equation can be rewritten as

$$\frac{\mathrm{d}^2 R^*}{\mathrm{d}r^2} + \frac{1}{r}\frac{\mathrm{d}R^*}{\mathrm{d}r} + \left[k_n^2\left(\frac{1}{\xi^2} - 1\right) - \frac{1}{r^2}\right]R^* = 0, \tag{A2}$$

where $R^* = R/r$. This equation is known as a Bessel equation, and the solution is of the form

$$R^*(r) = C_1 J_1(\alpha r) + C_2 Y_1(\alpha r), \tag{A3}$$

where

$$\alpha = \begin{cases} \sqrt{k_n^2\left(\dfrac{1}{\xi^2} - 1\right)} & \text{for } \xi^2 < 1 \\ i\sqrt{k_n^2\left(1 - \dfrac{1}{\xi^2}\right)} & \text{for } \xi^2 > 1 \end{cases} \tag{A4}$$

is the wave number inside the vortex core, J_1 is the first-order Bessel function of the first kind, while Y_1 is the first-order Bessel function of the second kind. Since ψ_1 must be finite at $r=0$, while $Y_1(0)=\infty$, we require $C_2=0$. The solution thus becomes

$$R(r) = \begin{cases} C_1 r J_1(\alpha r) & \text{for } \xi^2 < 1 \\ C_1 r I_1(i\alpha r) & \text{for } \xi^2 > 1. \end{cases} \tag{A5}$$

2. Exterior ($r>1$)

In the exterior of the vortex, the equation for $R^*(r)$ is

$$r^2\frac{\mathrm{d}^2R^*}{\mathrm{d}r^2} + r\frac{\mathrm{d}R^*}{\mathrm{d}r} - \left[1 - \frac{k_n^2}{\xi^2 \mathrm{N}^2\,\mathrm{Ro}} + k_n^2\left(1 - \frac{1}{\xi^2\mathrm{N}^2\,\mathrm{Ro}^2}\right)r^2\right]R^* = 0, \tag{A6}$$

which can be rewritten as

$$r^2\frac{\mathrm{d}^2R^*}{\mathrm{d}r^2} + r\frac{\mathrm{d}R^*}{\mathrm{d}r} - \left[\gamma^2 + \frac{\beta^2}{\mathrm{R_c^2}}r^2\right]R^* = 0, \tag{A7}$$

where R_c is the radius of the cylinder, $\gamma^2 = 1 - k_n^2/(\xi^2\mathrm{N}^2\,\mathrm{Ro})$, and $\beta^2 = k_n^2\mathrm{R_c^2}\{1 - [\xi(\mathrm{Ro}+1)]^{-2}\}$. Note that both γ and β can be either real or imaginary.

If $\xi^2 > (\mathrm{Ro}+1)^{-2}$, then we take $\beta = k_n\mathrm{R_c}\sqrt{1-[\xi(\mathrm{Ro}+1)]^{-2}} \in \mathbb{R}^+$, and Eq. (A7) can be solved in terms of the modified Bessel functions of order γ. For computational convenience we wish to construct two linearly independent solutions of Eq. (A7) that are real valued irrespective of $\gamma \in \mathbb{R}$ or $\gamma \in \mathbb{I}$. It is thus found that

$$R(r) = C_3 r K_\gamma(\beta r/\mathrm{R_c}) + C_4 r L_\gamma(\beta r/\mathrm{R_c}), \tag{A8}$$

where

$$L_\gamma(x) = \tfrac{1}{2}[I_\gamma(x) + I_{-\gamma}(x)]. \tag{A9}$$

I_γ and K_γ are the modified Bessel functions of order γ of the first and second kinds, respectively.

The boundary condition at the external wall requires $\psi(r=\mathrm{R_c})=0$, and hence

$$C_3 K_\gamma(\beta) + C_4 L_\gamma(\beta) = 0. \tag{A10}$$

For large values of β, $K_\gamma(\beta)\to 0$ while $L_\gamma(\beta)\to\infty$. In this case C_4 must be very small, and the solution can be largely simplified. Nonetheless, the complete solution will be presented here.

The solutions in the interior and the exterior have to be matched. Since the frequencies in the interior and the exterior are assumed to be the same, α must be related to β according to

$$\alpha^2 = \mathrm{N}^2\,\mathrm{Ro}^2\left(k_n^2 - \frac{\beta^2}{\mathrm{R_c^2}}\right) - k_n^2. \tag{A11}$$

In addition, continuity in ψ and $\partial\psi/\partial r$ should be imposed at $r=1$, which yields

$$C_1 = \frac{C_3}{J_1(\alpha)}\left[K\gamma(\beta/\mathrm{R_c}) - \frac{K_\gamma(\beta)}{L_\gamma(\beta)}L_\gamma(\beta/\mathrm{R_c})\right] \tag{A12}$$

and

$$\frac{\alpha J_0(\alpha)}{J_1(\alpha)} = \frac{\left.\frac{\partial}{\partial r}[rK_\gamma(\beta r/\mathrm{R_c})]\right|_{r=1} - \frac{K_\gamma(\beta)}{L_\gamma(\beta)}\left.\frac{\partial}{\partial r}[rL_\gamma(\beta r/\mathrm{R_c})]\right|_{r=1}}{K_\gamma(\beta/\mathrm{R_c}) - \frac{K_\gamma(\beta)}{L_\gamma(\beta)}L_\gamma(\beta/\mathrm{R_c})}. \tag{A13}$$

The latter equation is a transcendental equation for α, which can have several solutions, each of them corresponding to a different frequency ξ. For $\xi>1$, the left-hand side of this transcendental equation has to be replaced by $|\alpha|I_0(|\alpha|)/I_1(|\alpha|)$.

If $\xi<(\mathrm{Ro}+1)^{-2}$, $\beta = i\beta^*$ with $\beta^* = k_n\mathrm{R_c}\sqrt{[\xi(\mathrm{Ro}+1)]^{-2}-1} \in \mathbb{R}^+$, and Eq. (A7) can be written as

$$r^2\frac{\mathrm{d}^2R^*}{\mathrm{d}r^2} + r\frac{\mathrm{d}R^*}{\mathrm{d}r} + \left[\frac{\beta^{*2}}{\mathrm{R_c^2}}r^2 - \gamma^2\right]R^* = 0. \tag{A14}$$

The solution to Eq. (A14) can be written in terms of Bessel functions of the first and second kinds. Again, for computational convenience, we introduce the following two real-valued, linearly independent solutions:

$$B_\gamma(x) = \tfrac{1}{2}[J_\gamma(x) + J_{-\gamma}(x)] \tag{A15}$$

and

$$D_\gamma(x) = \tfrac{1}{2}[Y_\gamma(x) + Y_{-\gamma}(x)]. \tag{A16}$$

A solution of Eq. (A14) can then be written as

$$R(r) = C_3 r B_\gamma(\beta^* r/\mathrm{R_c}) + C_3 r D_\gamma(\beta^* r/\mathrm{R_c}). \tag{A17}$$

Applying the boundary condition at the external wall yields

$$C_4 = -C_3\frac{B_\gamma(\beta^*)}{D_\gamma(\beta^*)}, \tag{A18}$$

while continuity of ψ and $\partial\psi/\partial r$ at $r=1$ yields

$$C_1 = \frac{C_4}{J_1(\alpha)}\left[B\gamma(\beta^*/\mathrm{R_c}) - \frac{B_\gamma(\beta^*)}{D_\gamma(\beta^*)}D_\gamma(\beta^*/\mathrm{R_c})\right] \tag{A19}$$

and

$$\frac{\alpha J_0(\alpha)}{J_1(\alpha)} = \frac{\left.\frac{\partial}{\partial r}[rB_\gamma(\beta^* r/\mathrm{R_c})]\right|_{r=1} - \frac{B_\gamma(\beta^*)}{D_\gamma(\beta^*)}\left.\frac{\partial}{\partial r}[rD_\gamma(\beta^* r/\mathrm{R_c})]\right|_{r=1}}{B_\gamma(\beta^*/\mathrm{R_c}) - \frac{B_\gamma(\beta^*)}{D_\gamma(\beta^*)}D_\gamma(\beta^*/\mathrm{R_c})}, \tag{A20}$$

which is again a transcendental equation for α. Here too, if $\xi>1$, the left-hand side of this expression has to be replaced by $|\alpha|I_0(|\alpha|)/I_1(|\alpha|)$.

On the other hand, it can be seen that the expression cannot satisfy the boundary condition $R(r)\to 0$ as $r\to\infty$ because the Bessel functions decay like $r^{-1/2}$ as $r\to\infty$, and hence, $R(r)$ grows like $r^{1/2}$ as $r\to\infty$.

APPENDIX B: DECAY RATE FOR SMALL VERTICAL WAVELENGTH

If $\alpha_m \ll k_n$, horizontal diffusion can be neglected. Vertical diffusion does not modify the basic swirl flow if V_0 does not depend on z. However, diffusion affects the evolution of the perturbation. This can be expressed by including the vertical viscous terms in Eq. (18) for ψ_1

$$\frac{\partial^2 \tilde{\Delta}\psi_1}{\partial t^2} = -\frac{1}{\delta r^3 \mathrm{N}^2}\frac{\partial V_0^2}{\partial r}\frac{\partial^2 \psi_1}{\partial z^2} + \frac{2}{\mathrm{Re\,N}\delta^2}\frac{\partial^2}{\partial z^2}\frac{\partial \tilde{\Delta}\psi_1}{\partial t} - \frac{1}{\mathrm{N\,Re}^2\,\delta^4}\frac{\partial^4 \tilde{\Delta}\psi_1}{\partial z^4}. \tag{B1}$$

Stress-free boundary conditions are imposed at $z=0$ and $z=1$, and we assume a harmonic dependence both in time and in z: $\psi_1 = R(r)\sin(\lambda_n z)e^{i\phi t}$. Substitution of this solution into Eq. (B1) yields

$$\left(\phi - i\frac{k_n^2}{\mathrm{N\,Re}}\right)^2 \tilde{\Delta}\psi_1 = -\frac{1}{\delta r^3 \mathrm{N}^2}\frac{\partial V_0^2}{\partial r}\frac{\partial^2 \psi_1}{\partial z^2}, \tag{B2}$$

which can be transformed into Eq. (20) for the inviscid case by taking $\xi = \phi - ik_n^2/\mathrm{N\,Re}$, where ξ is again the frequency for the inviscid case. Therefore, the frequency for the viscous case is

$$\phi = \xi + i\frac{k_n^2}{\mathrm{N\,Re}}, \tag{B3}$$

where the imaginary part is a damping coefficient, which in dimensional units can be written as $\nu\lambda_n^2/H^2$. This damping rate is the slowest damping rate possible, since if radial diffusion is included, the damping rate would be higher and the radial shape of the recirculation cells would be modified.

[1] W. Thomson, *Mathematical and Physical Papers* (Cambridge University Press, Cambridge, England, 1910), Vol. 4, p. 152.
[2] E. J. Hopfinger, "Turbulence and waves in a rotating tank," Annu. Rev. Fluid Mech. **125**, 505 (1982).
[3] D. Fultz, "A note on overstability and the elastoid-inertia oscillations of Kelvin, Solberg, and Bjerknes," J. Atmos. Sci. **16**, 199 (1959).
[4] S. Arendt, D. Fritts, and O. Andreassen, "The initial value problem for Kelvin vortex waves," J. Fluid Mech. **344**, 181 (1997).
[5] D. Fabre, D. Sipp, and L. Jacquin, "Kelvin waves and the singular modes of the Lamb-Oseen vortex," J. Fluid Mech. **551**, 235 (2006).
[6] S. Le Dizès and L. Lacaze, "An asymptotic description of vortex Kelvin modes," J. Fluid Mech. **542**, 69 (2005).
[7] D. Sipp and L. Jacquin, "Widnall instabilities in vortex pairs," Phys. Fluids **15**, 1861 (2003).
[8] P. G. Saffman, *Vortex Dynamics* (Cambridge University Press, Cambridge, England, 1992).
[9] M. V. Melander and F. Hussain, "Core dynamics on a vortex column," Fluid Dyn. Res. **13**, 1 (1994).
[10] G. F. Carnevale, M. Briscolini, R. C. Kloosterziel, and G. K. Vallis, "Three-dimensionally perturbed vortex tubes in a rotating flow," J. Fluid Mech. **341**, 127 (1997).
[11] R. C. Kloosterziel, G. F. Carnevale, and P. Orlandi, "Inertial instability in rotating and stratified fluids: Barotropic vortices," J. Fluid Mech. **583**, 379 (2007).
[12] E. J. Hopfinger and G. J. F. van Heijst, "Vortices in rotating fluids," Annu. Rev. Fluid Mech. **25**, 241 (1993).
[13] S. Le Dizès, "Inviscid waves on a Lamb-Oseen vortex in a rotating stratified fluid: Consequences for the elliptic instability," J. Fluid Mech. **597**, 283 (2008).
[14] "COMSOL 3.5 User's Guide," COMSOL AB, Tegnérgatan 23, SE-111 40 Stockholm, Sweden, available as of May 2008 at http:\\www.comsol.com.
[15] M. P. Satijn, A. W. Cense, R. Verzicco, H. J. H. Clercx, and G. J. F. van Heijst, "Three-dimensional structure and decay properties of vortices in shallow fluid layers," Phys. Fluids **13**, 1932 (2001).
[16] R. A. D. Akkermans, L. P. J. Kamp, H. J. H. Clercx, and G. J. F. van Heijst, "Intrinsic three-dimensionality in electromagnetically driven shallow flows," Europhys. Lett. **83**, 24001 (2008).